Formulation and Analysis of Frequency- Dependent Boundaries in Finite-Difference Simulation with Compact Explicit Schemes

Forum Acusticum 2011 - Aalborg - Denmark

Formulation and Analysis of Frequency-Dependent Boundaries in Finite-Difference Simulation with Compact Explicit Schemes

Maarten van Walstijn
Sonic Arts Research Centre, School of Electronics, Electrical Engineering, and Computer Science, Queen's University Belfast, United Kingdom

Konrad Kowalczyk
Multimedia Communication and Signal Processing (LMS), University of Erlangen-Nuremberg, Germany

Summary
Compact explicit schemes are an attractive alternative to more conventional finite difference schemes such as Yee's classical staggered scheme, because they allow reducing the numerical dispersion error and increasing the effective bandwidth. In order to use these schemes for the simulation of room acoustics, numerical formulation of frequency-dependent absorbing boundaries is required. This paper presents such frequency-dependent boundary models, in which the wall impedance is represented with a digital filter. Structurally stable and efficient formulations are constructed by carefully combining the boundary condition with the compact explicit scheme. The formulation is general in that an arbitrary passive wall impedance can be defined, and numerical stability can be guaranteed without imposing any further constraint. The results include a comparison of predicted numerical reflection amplitudes for a number of important schemes in the parameterised family, including the standard rectilinear scheme, the interpolated digital waveguide mesh, and the interpolated wideband scheme. The analysis shows that the proposed boundary formulation is consistent with locally reacting surface theory, and that the boundary formulations generally display properties that are similar to that of the basic underlying scheme.

PACS no. 43.55.Ka,43.55.-n

1. Introduction

In room acoustics modelling, two distinct approaches dominate, namely geometrical and wave-based methods. In general, geometrical techniques (see [1] for a generalised formulation) are more efficient but the underlying assumption of approximating sound waves with sound rays is justified for high frequencies only [2]. In contrast, wave-based methods, that inherently model all wave-related phenomena, are typically accurate at lower frequencies. Accurate room acoustics prediction and auralisation thus requires using a wave-based method at sufficiently high sample rates or hybrid models that apply the two different approaches for different frequency bands [3].

Among wave-based methods, finite-differences are usually applied in the form of Yee's classical staggered grid method [4], originally employed in the room acoustics domain by Botteldooren in [5]. Obtaining accurate predictions with Yee's method requires heavy oversampling to reduce the numerical dispersion error, which for room modelling leads to enormous computational costs. The efficiency can in principle be improved using implicit schemes to reduce the dispersion error, thereby allowing the use of a much lower sample rate [6], but the implementation and boundary formulations for irregular room geometries present major difficulties for such schemes. Improving accuracy is also possible using higher-order spatial schemes (known as 'large star' systems), but then the treatment of boundaries becomes unwieldy. For this reason, this paper considers only compact explicit schemes. In addition, considerations are constrained here to nonstaggered 3-D compact schemes on a rectilinear stencil, allowing a straightforward fit of the grid to enclosures with mainly parallel walls, which are predominant in real architecture. As explained in [7], the family of compact explicit schemes captures many schemes used in previous studies, including the

Table I. List of specific compact explicit schemes and their associated parameters and coefficients. The listed values for λ indicate the Courant numbers used in practice, which for all schemes except the IDWM is chosen at the stability bound.

	Standard Leapfrog (SLF)	Octa-hedral (OCTA)	Cubic Close-Packed (CCP)	Interp. DWM (IDWM)	Interp. Isotropic (IISO)	Interp. Wideband (IWB)
a	0	$\frac{1}{2}$	$\frac{1}{4}$	0.2034	$\frac{1}{6}$	$\frac{1}{4}$
b	0	$\frac{1}{4}$	0	0.0438	$\frac{1}{48}$	$\frac{1}{16}$
λ	$\sqrt{\frac{1}{3}}$	1	1	$\sqrt{\frac{1}{3}}$	$\sqrt{\frac{3}{4}}$	1
d_1	$\frac{1}{3}$	0	0	0.1205	$\frac{15}{48}$	$\frac{1}{4}$
d_2	0	0	$\frac{1}{4}$	0.0386	$\frac{3}{32}$	$\frac{1}{8}$
d_3	0	$\frac{1}{4}$	0	0.0146	$\frac{1}{64}$	$\frac{1}{16}$
d_4	0	0	-1	0.6970	$-\frac{9}{8}$	$-\frac{3}{2}$

standard leapfrog (SLF) scheme [8] (which is also referred to as a standard rectilinear scheme, and has the same numerical dispersion as Yee's method), the octahedral scheme [9, 10], and the 3-D interpolated digital waveguide mesh (IDWM) [11] (see Table I).

The focus of this paper is on numerical formulation of frequency-dependent boundaries for compact explicit schemes. As shown in [12], one-port boundary terminations in digital waveguide mesh simulations using reflection coefficients or reflection filters (see e.g., [13, 14, 15]) are not consistent with locally reacting wall theory and may even cause instabilities. A better boundary formulation exists for Yee's method [5], but it is limited in the type of wall impedance that can be specified and it imposes an additional stability constraint. This paper presents a general approach to formulating a digital impedance filter (DIF) boundary model (originally proposed in [16] for the SLF scheme) that overcomes these problems and limitations.

2. Compact Explicit Schemes

Considering a 3-D Cartesian coordinate system x-y-z, sound wave propagation in air is governed by

$$\frac{\partial^2 p}{\partial t^2} = c^2 \left(\frac{\partial^2 p}{\partial x^2} + \frac{\partial^2 p}{\partial y^2} + \frac{\partial^2 p}{\partial z^2} \right), \tag{1}$$

where p is the acoustic pressure, t denotes time, and c is the wave velocity. Discretising space and time using a grid spacing X and a time step T, compact explicit schemes approximating (1) can be described by

$$\begin{aligned} \delta_t^2 p^n_{l,m,i} = \lambda^2 \Big[&\left(\delta_x^2 + \delta_y^2 + \delta_z^2\right) + b\, \delta_x^2 \delta_y^2 \delta_z^2 \\ &+ a \left(\delta_x^2 \delta_y^2 + \delta_y^2 \delta_z^2 + \delta_x^2 \delta_z^2\right) \Big] p^n_{l,m,i}, \end{aligned} \tag{2}$$

where $p^n_{l,m,i} \equiv p(x,y,z,t)\big|_{x=lX, y=mX, z=iX, t=nT}$, and

$$\delta_t^2 p^n_{l,m,i} \equiv p^{n+1}_{l,m,i} - 2p^n_{l,m,i} + p^{n-1}_{l,m,i}\,, \tag{3}$$
$$\delta_x^2 p^n_{l,m,i} \equiv p^n_{l+1,m,i} - 2p^n_{l,m,i} + p^n_{l-1,m,i}\,, \tag{4}$$
$$\delta_y^2 p^n_{l,m,i} \equiv p^n_{l,m+1,i} - 2p^n_{l,m,i} + p^n_{l,m-1,i}\,, \tag{5}$$
$$\delta_z^2 p^n_{l,m,i} \equiv p^n_{l,m,i+1} - 2p^n_{l,m,i} + p^n_{l,m,i-1}\,, \tag{6}$$

are second-order centered finite-difference operators. Applying these to (2) yields the generalised difference equation for compact explicit schemes:

$$\begin{aligned} p^{n+1}_{l,m,i} \;=\; & d_1 \big(p^n_{l+1,m,i} + p^n_{l-1,m,i} + p^n_{l,m+1,i} \\ & + p^n_{l,m-1,i} + p^n_{l,m,i+1} + p^n_{l,m,i-1} \big) \\ & + d_2 \big(p^n_{l+1,m+1,i} + p^n_{l+1,m-1,i} + p^n_{l+1,m,i+1} \\ & + p^n_{l+1,m,i-1} + p^n_{l,m+1,i+1} + p^n_{l,m+1,i-1} \\ & + p^n_{l,m-1,i+1} + p^n_{l,m-1,i-1} + p^n_{l-1,m+1,i} \\ & + p^n_{l-1,m-1,i} + p^n_{l-1,m,i+1} + p^n_{l-1,m,i-1} \big) \\ & + d_3 \big(p^n_{l+1,m+1,i+1} + p^n_{l+1,m-1,i+1} \\ & + p^n_{l+1,m+1,i-1} + p^n_{l+1,m-1,i-1} \\ & + p^n_{l-1,m+1,i+1} + p^n_{l-1,m-1,i+1} \\ & + p^n_{l-1,m+1,i-1} + p^n_{l-1,m-1,i-1} \big) \\ & + d_4\, p^n_{l,m,i} - p^{n-1}_{l,m,i}, \end{aligned} \tag{7}$$

with the parameterised coefficients

$$\begin{aligned} d_1 &= \lambda^2(1 - 4a + 4b), \quad d_2 = \lambda^2(a - 2b), \\ d_3 &= \lambda^2 b, \quad d_4 = 2(1 - 3\lambda^2 + 6\lambda^2 a - 4b\lambda^2). \end{aligned} \tag{8}$$

In the above equations, a and b denote free numerical parameters constrained by $a \leq \frac{1}{2}$, $b \geq \frac{1}{16}(12a - 3)$, and $\lambda = cT/X$ denotes the Courant number, which is commonly chosen at the stability bound [7]. A list of specific schemes [i.e. choice of (a, b)] with their respective implementation coefficient values is presented in Table I.

A number of important properties about any scheme within this family, namely the stability bound,

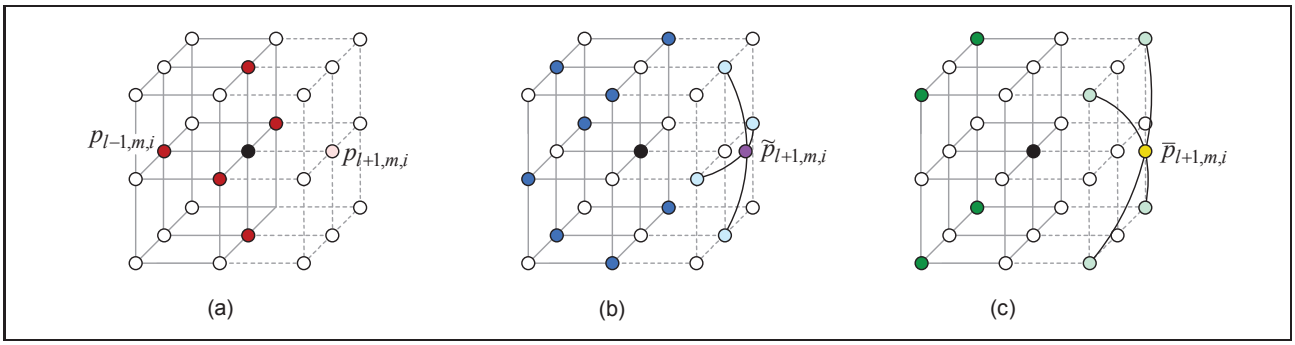

Figure 1. Pressure nodes of a compact explicit scheme at a boundary positioned as a plane of constant x, with the interior nodes on the lefthand-side of the boundary. In all three subfigures, the central black node indicates the update node $p_{l,m,i}$, and the lighter-version shades indicate a specific set of ghost-nodes. (a) Axial nodes highlighted with red, where the pink node indicates the ghost-node. (b) Side-diagonal nodes indicated with blue, where the purple node indicates the interpolated ghost-node. (c) Diagonal nodes indicated with green, where the yellow node indicates the interpolated ghost-node.

the numerical cut-off frequency, and the numerical disperion as a function of propagation angle and frequency, can be derived from (7) using a frequency-domain ansatz approach [7]. The main conclusions of this analysis are as follows. The IWDM and IISO scheme display a low dependence of the numerical disperion on direction, thus offering the possibility of applying frequency warping by pre- and post-processing, which allows recovering about half of the available spectrum with very low dispersion error [11]; if however a gradual increase in dispersion error with frequency is allowable, then the interpolated wideband (IWB) scheme is preferable, since it does not have a numerical cut-off below Nyquist, and generally suffers the least from numerical disperion effects. The IWB is therefore also a logical choice for dynamic on-line simulations, where frequency-warping cannot be used, and has shown to be about seven times more efficient than the SLF [7]. A similar analysis has previously been applied to the 2-D wave equation [17].

3. Boundary Formulation

For a locally reacting boundary perpendicular to the particle velocity in positive x-direction, the pressure at the boundary satisfies [12],

$$\frac{\partial p}{\partial t} = -c\,\xi_w\,\frac{\partial p}{\partial x}, \tag{9}$$

where $\xi_w = Z_w/\rho c$ is the specific wall impedance, that may be a function of frequency, and ρ and Z_w are the air density and the wall impedance, respectively. When both the boundary condition and the wave equation simultaneously apply at a boundary [12], the planar-wave reflection coefficient may be defined as a function of the angle of incidence [2]

$$R_{\theta,\phi} = \frac{\xi_w \cos\theta\cos\phi - 1}{\xi_w \cos\theta\cos\phi + 1}, \tag{10}$$

where θ and ϕ denote azimuth and elevation, respectively. For modelling frequency-dependent boundaries in the digital domain, the specific wall impedance is replaced with a digital impedance filter (DIF) $\xi(z)$, where z now denotes the z-transform variable. In order to ensure that $\xi(z)$ is positive real, first a passive digital reflection filter $R_{0,0}(z)$ - which matches reflection theory or data for a normal angle of incidence - is designed, and next the DIF is obtained by inverting (10) [16], yielding an IIR filter

$$\xi_w(z) = \frac{1+R_{0,0}(z)}{1-R_{0,0}(z)} = \frac{b_0 + \sum_{k=1}^{N} b_k z^{-k}}{a_0 + \sum_{k=1}^{N} a_k z^{-k}}, \tag{11}$$

where b_k and a_k are the DIF zero- and pole-coefficients. We may associate a specific input v^n and output w^n with the DIF and construct the IIR difference equation

$$w^n = \frac{1}{a_0}\left[b_0 v^n + \underbrace{\sum_{k=1}^{N}\left(b_k\, v^{n-k} - a_k\, w^{n-k}\right)}_{g^n}\right], \tag{12}$$

where g^n represents an intermediate 'history variable' that accounts for all past contributions associated with the specific input v^n.

Considering then a pressure node at the boundary in a room modeled with the discretised wave equation (7), there are nine grid points lying outside the modeled space [see Fig. 1(a-c)], which in the literature are often referred to as 'ghost points' [18]. These points must be eliminated from the discretised wave equation using the boundary condition. This elimination process can be divided into three steps: (I) for an axial ghost point, (II) for four side-diagonal ghost points, and (III) for four diagonal ghost points. Step (I) starts with discretising the boundary condition (9) with centered-difference operators, then transforming

to the z-domain, giving

$$P_{l,m,i}\left(z-z^{-1}\right) = \lambda \underbrace{\xi_w(z)\overbrace{\left(P_{l-1,m,i}-P_{l+1,m,i}\right)}^{V_a}}_{W_a}, \tag{13}$$

where we can immediately identify the associated (z-domain) axial input V_a and output W_a. By rearranging, using the z-transform of (12) and transforming back to the time domain, the following explicit formula for the axial ghost-node [see Fig. 1(a)] can be found:

$$p^n_{l+1,m,i} = p^n_{l-1,m,i} + \frac{a_0}{\lambda b_0}\left(p^{n-1}_{l,m,i} - p^{n+1}_{l,m,i}\right) + \frac{g^n_a}{b_0}, \tag{14}$$

where g_a denotes the history variable associated with the axial pressure-node term.

For step (II), we first apply a linear interpolation on side-diagonal grid points lying inside and outside of the modeled space [as depicted in Fig. 1(b)], which can be expressed as

$$\widetilde{p}^{\,n}_{l-1,m,i} = \frac{1}{4}\left(p^n_{l-1,m+1,i} + p^n_{l-1,m-1,i} + p^n_{l-1,m,i+1} + p^n_{l-1,m,i-1}\right), \tag{15}$$

$$\widetilde{p}^{\,n}_{l+1,m,i} = \frac{1}{4}\left(p^n_{l+1,m+1,i} + p^n_{l+1,m-1,i} + p^n_{l+1,m,i+1} + p^n_{l+1,m,i-1}\right), \tag{16}$$

where $\widetilde{p}_{l-1,m,i}$ and $\widetilde{p}_{l+1,m,i}$ are the pressure values at two interpolated nodes lying on the sphere that goes through all twelve side-diagonal nodes. In step (III), an analogous interpolation of diagonal inner and outer grid nodes yields

$$\overline{p}^{\,n}_{l-1,m,i} = \frac{1}{4}\left(p^n_{l-1,m+1,i+1} + p^n_{l-1,m-1,i+1} + p^n_{l-1,m+1,i-1} + p^n_{l-1,m-1,i-1}\right), \tag{17}$$

$$\overline{p}^{\,n}_{l+1,m,i} = \frac{1}{4}\left(p^n_{l+1,m+1,i+1} + p^n_{l+1,m-1,i+1} + p^n_{l+1,m+1,i-1} + p^n_{l+1,m-1,i-1}\right), \tag{18}$$

where $\overline{p}_{l-1,m,i}$ and $\overline{p}_{l+1,m,i}$ respectively are the pressure values at two interpolated diagonal nodes lying on the sphere that goes through all eight diagonal grid points, as illustrated in Fig. 1(c). Since the interpolated values are located across the boundary, the discrete boundary condition in the direction normal to the wall can again be applied, as in step (I), yielding

$$\widetilde{p}^{\,n}_{l+1,m,i} = \widetilde{p}^{\,n}_{l-1,m,i} + \frac{a_0}{\lambda b_0}\left(p^{n-1}_{l,m,i} - p^{n+1}_{l,m,i}\right) + \frac{g^n_{sd}}{b_0}, \tag{19}$$

$$\overline{p}^{\,n}_{l+1,m,i} = \overline{p}^{\,n}_{l-1,m,i} + \frac{a_0}{\lambda b_0}\left(p^{n-1}_{l,m,i} - p^{n+1}_{l,m,i}\right) + \frac{g^n_{d}}{b_0}, \tag{20}$$

where g_{sd} and g_d denote the history variable associated with the DIF input due to side-diagonal and diagonal pressure-node terms, respectively. Substituting (15-18) into (19-20), and using the resulting formulae together with (14) to eliminate for the nine ghost points in the discrete wave equation (7) then gives the final boundary update equation

$$\begin{aligned} p^{n+1}_{l,m,i} = {} & \frac{d_1}{d_0}\left(2p^n_{l-1,m,i} + p^n_{l,m+1,i} + p^n_{l,m-1,i} + p^n_{l,m,i+1} + p^n_{l,m,i-1}\right) + \\ & \frac{d_2}{d_0}\left(2p^n_{l-1,m+1,i} + 2p^n_{l-1,m-1,i} + 2p^n_{l-1,m,i+1} + 2p^n_{l-1,m,i-1} + p^n_{l,m+1,i+1} + p^n_{l,m+1,i-1} + p^n_{l,m-1,i+1} + p^n_{l,m-1,i-1}\right) + \\ & \frac{2d_3}{d_0}\left(p^n_{l-1,m+1,i+1} + p^n_{l-1,m-1,i+1} + p^n_{l-1,m+1,i-1} + p^n_{l-1,m-1,i-1}\right) + \\ & \frac{d_4}{d_0}p^n_{l,m,i} + \frac{\lambda^2}{d_0 b_0}\breve{g}^n + \left(\frac{\lambda a_0 - b_0}{d_0 b_0}\right)p^{n-1}_{l,m,i}, \end{aligned} \tag{21}$$

where $d_0 = (\lambda a_0 + b_0)/b_0$ and where the overall impedance filter input $\breve{v}^n$, filter output $\breve{w}^n$, and the intermediate value $\breve{g}^n$ are respectively defined as

$$\breve{v}^n = \frac{a_0}{\lambda b_0}\left(p^{n+1}_{l,m} - p^{n-1}_{l,m}\right) - \frac{\breve{g}^n}{b_0}, \tag{22}$$

$$\breve{w}^n = \frac{1}{a_0}\left(b_0\,\breve{v}^n + \breve{g}^n\right), \tag{23}$$

$$\breve{g}^n = \sum_{k=1}^{N}\left(b_k\,\breve{v}^{n-k} - a_k\,\breve{w}^{n-k}\right). \tag{24}$$

In the derivation above, the superposition property of linear systems was applied to group the history terms g_a, g_{sd}, and g_d into one overall history variable $\breve{g}$. The DIF model requires updating (21-24) in the order of presentation. Similar formulae can be derived for an opposite boundary and boundaries of constant y or constant z [7].

4. Numerical Boundary Analysis

The frequency-domain ansatz approach commonly used for analysing numerical stability and dispersion of finite-difference schemes may - provided that a consistent scheme is used - also be applied for the analysis of boundary formulations [12, 16, 17]. As shown in [7], applying such analysis to the boundary formulation discussed in the previous section yields the numerical reflection coefficient

$$\hat{R}_{\theta,\phi}(z) = -\frac{Q - G\,A}{Q - G\,A^{-1}}, \tag{25}$$

where $A = e^{j\hat{k}X\cos\theta\cos\phi}$, $B = e^{j\hat{k}X\sin\theta\cos\phi}$, $C = e^{j\hat{k}X\sin\phi}$, $\hat{k}$ the numerical wavenumber for a given direction (θ,ϕ), and the new variables are respectively given as

$$D = (B + B^{-1} + C + C^{-1}), \tag{26}$$

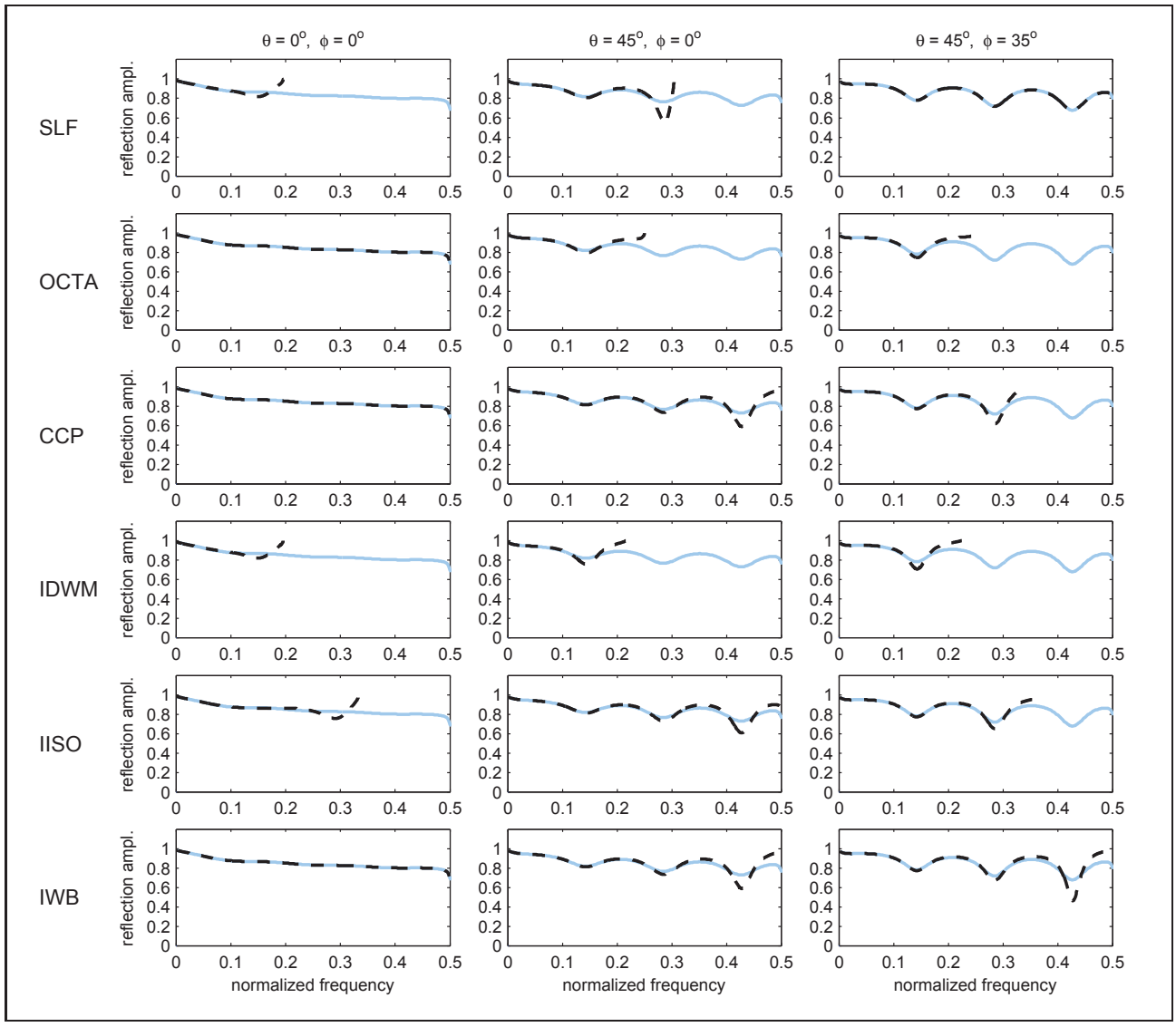

Figure 2. Numerical reflection amplitude (black dashed lines) of the fibrous material boundary with $d = 0.03$ and $\sigma = 200$ compared with theoretical reflection amplitude (blue solid lines) for the following angles of incidence ($\theta = 0^o, \phi = 0^o$), ($\theta = 45^o, \phi = 0^o$), and ($\theta = 45^o, \phi = 35^o$).

$$E = (BC + B^{-1}C + BC^{-1} + B^{-1}C^{-1}), \tag{27}$$

$$G = 2(d_1 + d_2 D + d_3 E), \tag{28}$$

$$Q = \frac{\lambda\left(z - z^{-1}\right)}{\xi_w(z)} + z + z^{-1} - d_1 D + d_2 E + d_4. \tag{29}$$

It can be shown analytically that $\left|\hat{R}_{\theta,\phi}(z)\right| \leq 1$ for any positive real digital impedance filter [7]. In other words, equation (21) renders a numerically stable boundary formulation for any physically feasible wall impedance.

Equation (25) allows investigating how the reflective behaviour in the simulation compares to theory. Since the largest and smallest errors always occur for one of the three extreme directions, the analysis is restricted to the following angles of incidence: normal incidence ($\theta = 0^o$, $\phi = 0^o$), side-diagonal incidence ($\theta = 45^o$, $\phi = 0^o$), and diagonal incidence ($\theta = 45^o$, $\phi = 35^o$). Fig. 2 shows the reflection amplitudes for various specific schemes modelling a boundary consisting of a layer of fibrous material and characterised by the impedance [19]

$$\xi_w(\omega) = \frac{Z_0(\omega)}{\rho c} \coth\left[\Gamma(\omega) d\right], \tag{30}$$

where the fibre thickness was chosen $d = 0.03m$ and where both $Z_0(\omega)$ and $\Gamma(\omega)$ depend on the flow resistivity, which was set at $\sigma = 200\text{Nsm}^{-4}$. Each plot is shown up to the numerical cutoff frequencies for the specific incidence and scheme. The results indicate that the global dependence of the reflection error on frequency is similar to that of the numerical dispersion of the underlying scheme. In accordance with findings for frequency-independent boundaries

[12], the error tends to decrease with impedance magnitude. Furthermore it can be seen that among the individual schemes, the boundary formulation is the most accurate when using the IWB scheme. The numerical reflection phase delay may also be assessed, and generally show a very tight fit with theory [7].

5. Concluding Remarks

A numerical model of frequency-dependent boundaries has been proposed. The formulation is compact, consistent with locally-reacting wall theory, does not impose an additional stability constraint, and allows stable simulation of rooms with arbitrary frequency-dependent wall impedances. As such, it represents a major improvement and extension on various previous boundary formulations in finite-difference modelling and related approaches to room acoustics simulation. A shown in [7], the approach is readily extended to modelling edges and corners, which is - unlike with Yee's scheme [5] - required when using compact explicit stencil.

Analysis of the numerical reflection coefficient with the numerical boundary analysis method allows a quick and reliable comparison between theory and simulation, avoiding the use of numerical experiments such as those applied in [12, 16] which are both elaborate and more prone to errors.

An important consequence of the consistency of scheme (used in the medium and at the boundary) is that frequency warping can for the first time be justifiably applied to responses obtained with finite-difference or digital waveguide mesh simulations of rooms with realistic boundaries.

One issue that has not been addressed so far, and could be of interest for future research, is whether a similar general digital impedance filter boundary model could developed for staggered grid methods.

References

[1] S. Siltanen, T. Lokki, L. Savioja, and C. Christensen, "The room acoustic rendering equation," *J. Acoustical Society America*, vol. 122, no. 3, pp. 1624–1635, 2007.

[2] H. Kuttruff, *Room Acoustics*, Applied Science Publishers Ltd, London, 1973.

[3] D.T. Murphy, M. Beeson, S. Shelley, A. Southern, and A. Moore, "RenderAIR - room acoustics simulation using a hybrid digital waveguide mesh," *Proc. 124th AES Convention*, May 17-20 2008, Amsterdam, The Netherlands.

[4] K.S. Yee, "Numerical solution of initial boundary value problems involving Maxwell's equations in isotropic media," *IEEE Trans. Antennas Propagat.*, vol. 14, pp. 302–307, 1966.

[5] D. Botteldooren, "Finite-difference time-domain simulation of low-frequency room acoustic problems," *J. Acoustical Society America*, vol. 98, no. 6, pp. 3302–3308, 1995.

[6] K. Kowalczyk and M. van Walstijn, "A comparison of nonstaggered compact FDTD schemes for the 3D wave equation," in *IEEE International Conference on Acoustics Speech and Signal Processing (ICASSP)*, , March 2010, pp. 197 –200.

[7] K. Kowalczyk and M. van Walstijn, "Room acoustics simulation using 3-D compact explicit FDTD schemes," *IEEE Transactions on Audio, Speech, and Language Processing*, vol. 19, pp. 34–46, 2011.

[8] J.C. Strikwerda, *Finite Difference Schemes and Partial Differential Equations*, Wadsworth & Brooks, Pacific Grove, CA, 1989.

[9] G.R. Campos and D.M. Howard, "On the computational efficiency of different waveguide mesh topologies for room acoustic simulation," *IEEE Trans. Speech and Audio Processing*, vol. 13, no. 5, pp. 1063–1072, September 2005.

[10] S. Bilbao and J.O. Smith, "Finite difference schemes and digital waveguide networks for the wave equation: Stability, passivity, and numerical dispersion," *IEEE Trans. Speech and Audio Processing*, vol. 11, pp. 255–266, May 2003.

[11] L. Savioja and V. Välimäki, "Interpolated rectangular 3-D digital waveguide mesh algorithms with frequency warping," *IEEE Trans. Speech and Audio Processing*, vol. 1, no. 6, pp. 738–790, November 2003.

[12] K. Kowalczyk and M. van Walstijn, "Formulation of locally reacting surfaces in FDTD/K-DWM modelling of acoustic spaces," *Acta Acustica united with Acustica*, vol. 94, no. 6, pp. 891–906, 2008.

[13] J. Huopaniemi, L. Savioja, and M. Karjalainen, "Modeling of reflections and air absorption in acoustical spaces - a digital filter design approach," *Proc. IEEE Workshop on Appl. of Signal Processing to Audio and Acoustics (WASPAA)*, pp. 1–4, October 1997, New Palz, NY.

[14] A. Kelloniemi, "Frequency-dependent boundary condition for the 3-D digital waveguide mesh," *Proc. Int. Conf. Digital Audio Effects (DAFx'06)*, pp. 161–164, September 2006, Montreal, Canada.

[15] D.T. Murphy and M. Beeson, "The KW-boundary hybrid digital waveguide mesh for room acoustics applications," *Trans. on Audio, Speech and Language Processing*, vol. 12, no. 2, pp. 552–564, 2007.

[16] K. Kowalczyk and M. van Walstijn, "Modeling frequency-dependent boundaries as digital impedance filters in FDTD and K-DWM room acoustics simulations," *J. Audio Eng. Soc.*, vol. 56, no. 7/8, pp. 569–583, 2008.

[17] K. Kowalczyk and M. van Walstijn, "Wideband and isotropic room acoustics simulation using 2-D interpolated FDTD schemes," *IEEE Transactions on Audio, Speech, and Language Processing*, vol. 18, no. 1, pp. 78 –89, 2010.

[18] J.W. Thomas, *Numerical Partial Differential Equations: Finite Difference Methods*, Springer-Verlag, New York, 1998.

[19] J.-F. Allard and Y. Champoux, "New empirical equations for sound propagation in rigid frame fibrous materials," *J. Acoustical Society America*, vol. 91, no. 6, pp. 3346–3353, 1992.